REPORT DOCUMENTATION PAGE

Form Approved OMB NO. 0704-0188

1. REPORT DATE (DD-MM-YYYY)	2. REPORT TYPE	3. DATES COVERED (From - To)
17-08-2015	Final Report	11-Aug-2014 - 10-May-2015

4. TITLE AND SUBTITLE
Final Report: Selective Metallothermal Reactions for Ceramic Matrix Nanocomposites

5a. CONTRACT NUMBER
W911NF-14-1-0560

5b. GRANT NUMBER

5c. PROGRAM ELEMENT NUMBER
611102

6. AUTHORS
David W. Lipke

5d. PROJECT NUMBER

5e. TASK NUMBER

5f. WORK UNIT NUMBER

7. PERFORMING ORGANIZATION NAMES AND ADDRESSES
Alfred University
1 Saxon Drive

Alfred, NY 14802 -1205

8. PERFORMING ORGANIZATION REPORT NUMBER

9. SPONSORING/MONITORING AGENCY NAME(S) AND ADDRESS (ES)
U.S. Army Research Office
P.O. Box 12211
Research Triangle Park, NC 27709-2211

10. SPONSOR/MONITOR'S ACRONYM(S)
ARO

11. SPONSOR/MONITOR'S REPORT NUMBER(S)
66087-MS-II.1

12. DISTRIBUTION AVAILIBILITY STATEMENT
Approved for Public Release; Distribution Unlimited

13. SUPPLEMENTARY NOTES
The views, opinions and/or findings contained in this report are those of the author(s) and should not contrued as an official Department of the Army position, policy or decision, unless so designated by other documentation.

14. ABSTRACT
Research activities supported by a nine-month Short Term Innovative Research (STIR) grant from the Army Research Office, Materials Science Division, Synthesis and Processing of Materials Program are disclosed herein, comprising: synthesis of selected mixed oxide and non-oxide ceramic solid solution powders via conventional solid state techniques; gas-solid reaction processing to produce ceramic nanocomposite particles; and, on a limited basis, bulk consolidation via spark plasma sintering. Microstructural characterization of products was conducted via electron microscopy and x-ray diffraction.

15. SUBJECT TERMS
reaction processing, ceramic, composite, internal precipitation, selective reduction

16. SECURITY CLASSIFICATION OF:			17. LIMITATION OF ABSTRACT	15. NUMBER OF PAGES	19a. NAME OF RESPONSIBLE PERSON
a. REPORT	b. ABSTRACT	c. THIS PAGE			David Lipke
UU	UU	UU	UU		19b. TELEPHONE NUMBER 607-871-2729

Report Title

Final Report: Selective Metallothermal Reactions for Ceramic Matrix Nanocomposites

ABSTRACT

Research activities supported by a nine-month Short Term Innovative Research (STIR) grant from the Army Research Office, Materials Science Division, Synthesis and Processing of Materials Program are disclosed herein, comprising: synthesis of selected mixed oxide and non-oxide ceramic solid solution powders via conventional solid state techniques; gas-solid reaction processing to produce ceramic nanocomposite particles; and, on a limited basis, bulk consolidation via spark plasma sintering. Microstructural characterization of products was conducted via electron microscopy and x-ray diffraction.

Exploratory work in the Ti-W-C, Al-Cr-O, and Ti-Nb-(B,C,N,O) systems has shown that selective metallothermal reactions may readily proceed via gaseous intermediates. Thermodynamic driving forces for second phase precipitation via gas-solid reaction appear to be analogous to those observed in the solid-state, resulting in similar reduction pathways. Selective gas-solid metallothermal reactions represent a significant advancement in processing science that, coupled with a better understanding of structure-processing relationships, is expected to result in unprecedented microstructural control of metal dispersion-strengthened ceramic nanocomposites.

Enter List of papers submitted or published that acknowledge ARO support from the start of the project to the date of this printing. List the papers, including journal references, in the following categories:

(a) Papers published in peer-reviewed journals (N/A for none)

Received Paper

TOTAL:

Number of Papers published in peer-reviewed journals:

(b) Papers published in non-peer-reviewed journals (N/A for none)

Received Paper

TOTAL:

Number of Papers published in non peer-reviewed journals:

(c) Presentations

Number of Presentations: 0.00

Non Peer-Reviewed Conference Proceeding publications (other than abstracts):

Received Paper

TOTAL:

Number of Non Peer-Reviewed Conference Proceeding publications (other than abstracts):

Peer-Reviewed Conference Proceeding publications (other than abstracts):

Received Paper

TOTAL:

Number of Peer-Reviewed Conference Proceeding publications (other than abstracts):

(d) Manuscripts

Received Paper

TOTAL:

Number of Manuscripts:

Books

Received Book

TOTAL:

Received	Book Chapter

TOTAL:

Patents Submitted

Patents Awarded

Awards

Graduate Students

NAME	PERCENT_SUPPORTED	Discipline
Robert J. Locker	1.00	
FTE Equivalent:	**1.00**	
Total Number:	**1**	

Names of Post Doctorates

NAME	PERCENT_SUPPORTED
FTE Equivalent:	
Total Number:	

Names of Faculty Supported

NAME	PERCENT_SUPPORTED	National Academy Member
David W. Lipke	0.00	
FTE Equivalent:	**0.00**	
Total Number:	**1**	

Names of Under Graduate students supported

NAME	PERCENT_SUPPORTED
FTE Equivalent:	
Total Number:	

Student Metrics

This section only applies to graduating undergraduates supported by this agreement in this reporting period

The number of undergraduates funded by this agreement who graduated during this period: 0.00

The number of undergraduates funded by this agreement who graduated during this period with a degree in science, mathematics, engineering, or technology fields:..... 0.00

The number of undergraduates funded by your agreement who graduated during this period and will continue to pursue a graduate or Ph.D. degree in science, mathematics, engineering, or technology fields:..... 0.00

Number of graduating undergraduates who achieved a 3.5 GPA to 4.0 (4.0 max scale):..... 0.00

Number of graduating undergraduates funded by a DoD funded Center of Excellence grant for Education, Research and Engineering:..... 0.00

The number of undergraduates funded by your agreement who graduated during this period and intend to work for the Department of Defense 0.00

The number of undergraduates funded by your agreement who graduated during this period and will receive scholarships or fellowships for further studies in science, mathematics, engineering or technology fields: 0.00

Names of Personnel receiving masters degrees

NAME

Total Number:

Names of personnel receiving PHDs

NAME

Total Number:

Names of other research staff

NAME PERCENT_SUPPORTED

FTE Equivalent:
Total Number:

Sub Contractors (DD882)

Inventions (DD882)

Scientific Progress

See attachment.

Technology Transfer

Selective Metallothermal Reactions for Ceramic Matrix Composites
FINAL REPORT
For the Period: August 11th, 2014 to May 10th, 2015

to U.S. Army – Army Research Office

Award No. **W911NF-14-1-0560** (Program Officer: Dr. David M. Stepp)

Date of Submission: August 17th, 2015

Principal Investigator (PI):
David W. Lipke
Assistant Professor
Kazuo Inamori School of Engineering
New York State College of Ceramics at Alfred University
Alfred, NY 14802
Email: Lipke@alfred.edu Phone: 607-871-2729

Recipient Organization:
Alfred University, Alfred, NY 14802
DUNS: 172257412

PI Signature: 

Executive Summary

Research activities supported by a nine-month Short Term Innovative Research (STIR) grant from the Army Research Office, Materials Science Division, Synthesis and Processing of Materials Program are disclosed herein, comprising: synthesis of selected mixed oxide and non-oxide ceramic solid solution powders via conventional solid state techniques; gas-solid reaction processing to produce ceramic nanocomposite particles; and, on a limited basis, bulk consolidation via spark plasma sintering. Microstructural characterization of products was conducted via electron microscopy and x-ray diffraction.

Exploratory work in the Ti-W-C, Al-Cr-O, and Ti-Nb-(B,C,N,O) systems has shown that selective metallothermal reactions may readily proceed via gaseous intermediates. Thermodynamic driving forces for second phase precipitation via gas-solid reaction appear to be analogous to those observed in the solid-state, resulting in similar reduction pathways. Selective gas-solid metallothermal reactions represent a significant advancement in processing science that, coupled with a better understanding of structure-processing relationships, is expected to result in unprecedented microstructural control of metal dispersion-strengthened ceramic nanocomposites.

Table of Contents

List of Figures

List of Tables

Introduction

Metal dispersion is an established method for strengthening and toughening ceramics.[1-5] Nevertheless, considerable disagreement pervades the associated literature concerning the origins of said improvements in ceramic nanocomposites, especially with regards to fracture toughness. While some researchers point to surface residual stresses from machining operations as the basis of apparent toughening in ceramic nanocomposites,[6-8] other researchers have argued that thermal mismatch stresses, grain size refinement, or various crack wake interactions are responsible for measured toughness increments.[9-24] Further compounding the issue is disagreement concerning the roles of intergranular versus intragranular reinforcements.[25-30]

Ambiguity lingers in large part due to a lack of robust synthesis and processing techniques to tailor microstructure of ceramic nanocomposites that would allow for methodological variation of features such as matrix and dispersed particle size distributions, volume fractions, microstructural locations, and thermophysical properties. Conventional methods to introduce dispersed second phase particles include traditional powder processing techniques and selective reduction of mixed oxide solid solutions and compounds.[31-39] The former typically involves blending powders, forming into desired shapes, sintering, and post-machining. A homogeneous mixture can be quite difficult to achieve depending on the nature of the blended powders (e.g., tendencies to agglomerate or segregate). Further, grain boundary pinning by fine dispersed particles can inhibit particle occlusion, leading to predominantly intergranular morphologies. Although not broadly applicable, clever researchers have been able to circumvent this issue by leveraging relatively uninhibited grain boundary movement during matrix recrystallization to envelop fine dispersed second phase particles, resulting in ceramic nanocomposites with a significant fraction of intragranular reinforcing phase.[29,30]

The second established method to introduce fine dispersed metal particles in ceramic matrices, called internal reduction, has historically been practiced exclusively on oxide-based solid solutions or compounds. Internal reduction is a subset of partial or selective reduction reactions that result from equilibration against an oxygen partial pressure that lies between the stability thresholds of its labile and noble constituents. Internal reduction microstructures are dictated by precipitation kinetics: small volume fractions of the labile solid solution constituent and fast bulk oxygen diffusion promote the formation of discrete particles whereas large volume fractions and slow bulk diffusion tend to promote interconnectivity of precipitates whose resultant morphologies may range from lamellar structures to contiguous domains. Anisotropic diffusion in the host lattice and fast diffusion pathways can further lead to non-equiaxed discrete precipitates and/or exaggerated precipitate growth along grain boundaries (i.e., discontinuous coarsening), respectively. It is thus challenging to sufficiently control internal reduction processes to be utilized as a means to synthesize metal dispersion-strengthened ceramic nanocomposites with tailored microstructures. Further, to date there has not been demonstrated a robust method to generalize the internal reduction concept to include non-oxide ceramic matrices.

Description of the Need

In their work on a specialized technique to produce intragranular reinforced alumina via recrystallization-occlusion of SiC nanoparticles, Piciacchio, Lee, and Messing conclude:

> "In addition to the reported mechanical property improvements in "nanocomposites," an intragranular microstructure could be effective in improving high-temperature oxidation resistance of the SiC phase because oxygen lattice diffusion in alumina is an order of magnitude lower than that of oxygen grain boundary diffusion. Although intragranular nanocomposites appear to be an interesting subclass of particulate composites, there are few guiding principles concerning their fabrication. Particulate composites with microstructures ranging from completely intergranular to completely intragranular and with different matrix and second-phase grain sizes would be useful for quantifying the relationship between reinforcement location and physical properties." [29]

Material designers as yet do not possess the necessary tools to independently vary important microstructural features such as matrix and reinforcement size, shape, location, and identity. This project seeks to redress this limitation by demonstrating an innovative processing paradigm proof-of-concept that combines reaction-based synthesis with traditional ceramic powder processing techniques to achieve an unprecedented degree of microstructural tailoring in metal dispersion-strengthened ceramic matrix composites.

A new approach advocated by the PI employs gas-phase mediated selective metallothermal reactions to internally precipitate secondary phases, resulting in a pseudo-intragranular morphology as depicted schematically below:

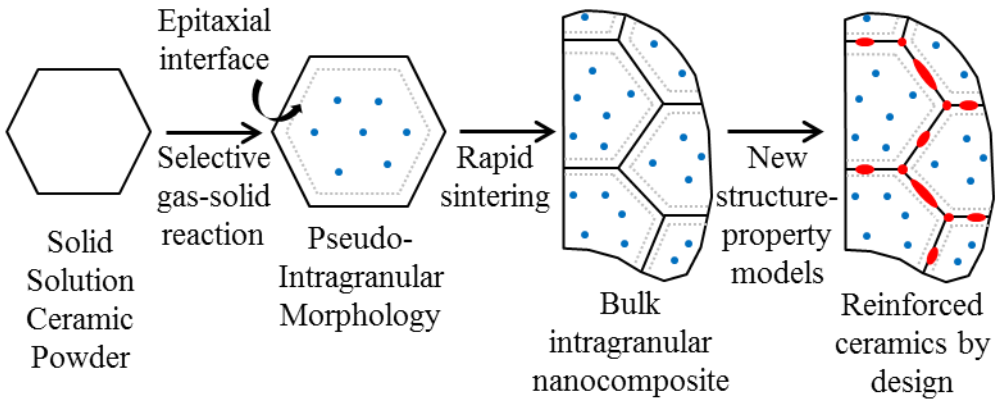

Figure 1: Schematic reaction processing scheme to independently control intergranular and intragranular reinforcement site fractions.

For example, suppose that the solid solution ceramic (MM′)X comprises a thermodynamically noble solvent MX and a thermodynamically labile solute M′X, such that upon exposure to excess metal M the following net reaction may occur:

$$(M_\delta M'_{1-\delta})X + (1-\delta)M = (1-\delta)(M')_{precipitate} + (MX)_{matrix}$$

where X typically comprises one or more of the following elements: B, C, N, O. The same reaction can be rewritten as:

$$(1-\delta)\{M'X\} + (1-\delta)M = (1-\delta)(M')_{precipitate} + (1-\delta)(MX)_{matrix}$$

where the { } brackets denote a solution component.

Project Goals

The primary research goals of this Short Term Innovative Research (STIR) project are: (a) to validate the feasibility of synthesizing ceramic nanocomposite powders; and, (b) to demonstrate bulk retention of nanostructures upon consolidation. The original proposal further sought to evaluate the following statements:

1. Gaseous disproportionation reactions (e.g., as exemplified by pack cementation- based techniques) are thermodynamically equivalent to solid state metallothermal reduction reactions.
2. Gaseous disproportionation reactions with (MM′)X-type solid solutions under conditions such that $D_X >> D_M, D_{M'}$ can induce internal phase transformations resulting in intragranular nanocomposite morphologies.
3. Intragranular nanocomposite powders can be consolidated with bulk retention of nanostructures via spark plasma sintering.
4. Ductile particle reinforced ceramic matrix nanocomposites with intragranular reinforcement locations can exhibit superior fracture toughness compared to nanocomposites with intergranular reinforcement locations for the same volume fraction of reinforcements.

At the completion of this nine-month effort, strong supporting experimental evidence in support of hypotheses (1), (2), and (3) has been found. These findings are detailed in the following sections. Due to difficulties in powder production scale up, specimens for mechanical properties evaluations could not be fabricated within the allotted project period. Any results from mechanical property testing upon current materials would be of suspect value due to the inhomogeneous nature of bulk consolidated ceramic nanocomposite microstructures thus produced at this early stage. Therefore, additional work improving the quality of starting materials and reaction processing apparatus will be required in order to evaluate hypothesis (4), as recommended in the future outlook section.

Experimental Methods

Materials Processing

The following tables summarize the processing steps involved in the production of selected mixed oxide and non-oxide ceramic solid solution powders.

Table 1: $(Al,Cr)_2O_3$ processing summary

Starting materials	α-Al_2O_3 (Ceralox HPA-0.5, 99.99%), Cr_2O_3 (Fisher Chemical, >99%), Iodine (Acros resublimed, 99.5%), Aluminum (Acros, 99%, 200 mesh), Alumina (Fisher Scientific, > 97.5%)
Calcining and jar milling	Starting materials were calcined to determine moisture content and the weights of corresponding batches were adjusted to compensate for moisture content. Starting materials were then jar milled in 250 mL HDPE Nalgene bottles in denatured ethanol for 8 hours with 0.4 wt. % Ferro 1150 modifier added as a pseudo-dispersant. Magnesia-stabilized zirconia media were used to agitate and mix the slurry.
Homogenization heat treatment	Mixed slurries were pan dried in air at 70°C overnight in a forced air oven and loaded into Al_2O_3 crucibles with lids for calcination. Heat treatment was performed by ramping materials to 600°C at 2°C/min., held at 600°C for 12 hours, then ramped to 1400°C at 5°C/min. with a 10 hour dwell time. The furnace was then cooled at 10°C/min. to room temperature.
Grinding and comminution	Resultant materials were sequentially comminuted via automated mortar and pestle grinding (Retsch RM100) and high energy planetary ball milling (Retsch PM200) in 125 mL alumina jars using 5 mm diameter 99.9% purity alumina media in deionized water for 45 minutes at 450 rpm. Resultant materials were pan dried at 150°C in vacuum drying oven at 100mBar.
Reaction processing	Reactants with nominal batch composition 0.24 g aluminum powder and 2.0 g $(Al_{0.81}Cr_{0.19})_2O_3$ were pressed into 0.5 inch diameter pellets under 1000-5000 lb applied load. The pellet was heat treated within a retort furnace (CM 1212 FL) by ramping under flowing argon to 1000°C at a rate of 5°C/min, with a dwell time of 24 hr, and cooling rate of 10°C/min. Reactants with nominal batch composition 0.30 g aluminum, 0.57 g alumina filler, 1.5 g $(Al_{0.81}Cr_{0.19})_2O_3$, and 0.22 g iodine were sealed under vacuum within a fused silica ampoule and heat treated at 1000°C for 24 hours. Reaction products were removed from the ampoule and thoroughly washed with deionized water and a stock sodium sulfate solution to remove iodine impurities.

Table 2: (Ti,W)C processing summary

Starting materials	$(Ti_{0.77}W_{0.23})C$ (H.C. Starck HV 100, 99.99%), Iodine (Acros resublimed, 99.5%), Titanium sponge (Sigma Aldrich, 3-19 mm, 99.5% trace metals basis)
Reaction processing	Reactants with nominal batch composition 0.75 g titanium powder and 2.0 g $(Ti_{0.77}W_{0.23})C$ were pressed into 0.5 inch diameter pellets under 1000-5000 lb applied load. The pellet was heat treated within a retort furnace (CM 1212 FL) by ramping under flowing argon to 1000°C at a rate of 5°C/min, with a dwell time of 24 hr, and cooling rate of 10°C/min. Starting materials were used as-received. Reactants with nominal batch composition 0.75 g titanium sponge, 2.0 g $(Ti_{0.77}W_{0.23})C$, and 0.35-0.80 g iodine were sealed under vacuum within a fused silica ampoule and heat treated at 1000°C for 24 hours. Reaction products were removed from the ampoule and thoroughly washed with deionized water and a stock sodium sulfate solution to remove iodine impurities.

Table 3: (Ti,Nb)C processing summary

Starting materials	TiC (Atlantic Equipment Engineers, 99.9%, 325 mesh), NbC (Atlantic Equipment Engineers, 99.8%, 325 mesh), Titanium powder (Alfa Aesar, 99%, 325 mesh)
Jar milling	Starting materials were jar milled in 250 mL HDPE Nalgene bottles in deionized water. Magnesia-stabilized zirconia media were used to agitate and mix the slurry.
Homogenization heat treatment	Mixed slurries were pan dried in air at 70°C overnight in a forced air oven. Heat treatment was performed in a Mellen Company, Inc. graphite element furnace (gratis access generously provided by Corning Incorporated) at 2100°C for 24 hours under vacuum atmosphere.
Grinding and comminution	Resultant materials were comminuted via high energy planetary ball milling (Retsch PM200) in 125 mL alumina jars using 5 mm 99.9% purity alumina media in deionized water for 45 minutes at 450 rpm. Resultant materials were pan dried at 150°C in a vacuum drying oven at 100mBar.
Reaction processing	Reactants with nominal batch composition 1.17 g titanium powder and 4.83 g (TiNb)C were pressed into 0.5 inch diameter pellets under 1000-5000 lb applied load. The pellet was heat treated within a retort furnace (CM 1212 FL) by ramping under flowing argon to 1000°C at a rate of 5°C/min, with a dwell time of 24 hr, and cooling rate of 10°C/min.

Table 4: (Ti,Nb)N processing summary

Starting materials	TiN (Alfa Aesar, 99.5%, -325 mesh), NbN (Alfa Aesar, 99.5%, -325 mesh), Iodine (Acros resublimed, 99.5%), Titanium powder (Alfa Aesar, 99%, 325 mesh), Titanium sponge (Sigma Aldrich, 3-19 mm, 99.5% trace metals basis)
Jar milling	Starting materials were jar milled in 250 mL HDPE Nalgene bottles in ethanol. Magnesia-stabilized zirconia media were used to agitate and mix the slurry.
Homogenization heat treatment	Mixed slurries were pan dried in air at 70°C overnight in a vacuum oven at 100 mBar and placed on an 99.8% alumina setter plate for heat treatment. Heat treatment was performed in a $MoSi_2$ element tube furnace at 1500°C for 36 hours under flowing nitrogen.
Grinding and comminution	Resultant materials were ground to fineness in mortar and pestle.
Reaction processing	Three experiments were run. The first experiment run was 2X excess Ti metal. 0.39g Ti metal was mixed with 2.5g $(Ti_{0.89}Nb_{0.11})N$ and pressed into a 0.25 inch pellet. The pellet was heat treated in a retort furnace (CM 121 FL) by ramping under flowing argon at 5C/min to 800C with a dwell time of 8 days then cooled at a rate of 10C/min. Second, the same amount of excess Ti metal was run (0.39g Ti metal was mixed with 2.5g $(Ti_{0.89}Nb_{0.11})N$ and pressed into a 0.25 inch pellet) but at 1000C for 24 hours. The third experiment was run with 5X excess Ti metal. 0.975g of Ti metal was added to 2.5g $(Ti_{0.89}Nb_{0.11})N$ and pressed into a 0.25 inch pellet. The pellet was heat treated at 1000C for 24 hours using the same ramp rates.

Table 5: $(Ti,Nb)B_2$ processing summary

Starting materials	TiB_2 (Atlantic Equipment Engineers, 99.7%, 10 μm APS), NbB_2 (Atlantic Equipment Engineers, 99.8%, 325 mesh), Iodine (Acros resublimed, 99.5%), Titanium powder (Alfa Aesar, 99%, 325 mesh), Titanium sponge (Sigma Aldrich, 3-19 mm, 99.5% trace metals basis)
Jar milling	Starting materials were jar milled in 250 mL HDPE Nalgene bottles in deionized water. Magnesia-stabilized zirconia media were used to agitate and mix the slurry.
Homogenization heat treatment	Mixed slurries were pan dried in air at 70°C overnight in a forced air oven. Heat treatment was performed in a Mellen Company, Inc. graphite element furnace (gratis access generously provided by Corning Incorporated) at 2100°C for 24 hours under vacuum atmosphere.
Grinding and comminution	Resultant materials were comminuted via high energy planetary ball milling (Retsch PM200) in 125 mL alumina jars using 5 mm 99.9% purity alumina media in deionized water for 45 minutes at 450 rpm. Resultant materials were pan dried at 150°C in a vacuum drying oven at 100mBar.
Reaction processing	Reactants with nominal batch composition 1.26-3.15 g titanium powder and 4.73-2.84 g $(TiNb)B_2$ were pressed into 0.5 inch diameter pellets under 1000-5000 lb applied load. The pellet was heat treated within a retort furnace (CM 1212 FL) by ramping under flowing argon to 1000°C at a rate of 5°C/min, with a dwell time of 24 hr, and cooling rate of 10°C/min.

Table 6: $(Ti,Nb)O_2$ processing summary

Starting materials	TiO_2 (rutile) (Alfa Aesar, 99.8%, 0.9-1.6 µm APS), Nb_2O_5 (Alfa Aesar, 99.5%, 100 mesh), Iodine (Acros resublimed, 99.5%), Titanium powder (Alfa Aesar, 99%, 325 mesh), Titanium sponge (Sigma Aldrich, 3-19 mm, 99.5% trace metals basis)
Jar milling	Starting materials were jar milled in 250 mL HDPE Nalgene bottles in deionized water. Magnesia-stabilized zirconia media were used to agitate and mix the slurry.
Homogenization heat treatment	Mixed slurries were pan dried in air at 70°C overnight in a vacuum oven at 100 mBar and placed on an 99.8% alumina setter plate for heat treatment. Heat treatment was performed in a Lindberg tube furnace at 1350°C for 24 hours under flowing 4% H_2/Ar atmosphere.
Grinding and comminution	Resultant materials were comminuted via high energy planetary ball milling (Retsch PM200) in 125 mL alumina jars using 5 mm 99.9% purity alumina media in deionized water for 45 minutes at 450 rpm. Resultant materials were pan dried at 150°C in a vacuum drying oven at 100mBar.
Reaction processing	Reactants with nominal batch composition 0.79 g titanium powder and 5.2 g $(Ti_{0.81}Nb_{0.19})O_2$ were pressed into 0.5 inch diameter pellets under 1000-5000 lb applied load. The pellet was heat treated within a retort furnace (CM 1212 FL) by ramping under flowing argon to 1000°C at a rate of 5°C/min, with a dwell time of 24 hr, and cooling rate of 10°C/min. Reactants with nominal batch composition 0.2 g titanium sponge, 1.50 g $(Ti_{0.81}Nb_{0.19})O_2$, and 0.25 g iodine were sealed under vacuum within a fused silica ampoule and heat treated at 1000°C for 24 hours. Reaction products were removed from the ampoule and thoroughly washed with deionized water and a stock sodium sulfate solution to remove iodine impurities.

Ampoule Sealing Procedure

Sealed reaction vessels were produced by pre-forming a crude crucible with a base stem out of fused silica/quartz glass (10.5 mm I.D x 12.75 mm O.D, Technical glass products, > 99.99% SiO2, OH < 5ppm), and loading in the titanium sponge or Al/Al_2O_3 powder mixture at the bottom of the crucible. The reactant powder was then added; in the case of the Ti reactions the powder was added in around the sponge by manual shaking, in the case of the Al reaction the reactant material was added as a separate layer on top of the Al/Al_2O_3 mix. The crucible was placed in the 0.5 inch quartz tube, pre-sealed at one end, then crystals of iodine pre-cooled to 0°C were placed into the vessel immediately prior to placement on the vacuum. The vessel was connected to vacuum via a 0.5 inch Ultra-torr fitting with Viton O-ring. The vessel was evacuated slowly by manipulation of air flow with a needle valve, and powder activity was

visually monitored to ensure remnant gas pressure in the powder didn't cause powder venting into the vacuum. After the ampoule was evacuated to the limits of a rotary vane pump, nominally 2 mTorr, the ampule was sealed by circumferential heating with an oxy-propane torch. The figure below illustrates the setup:

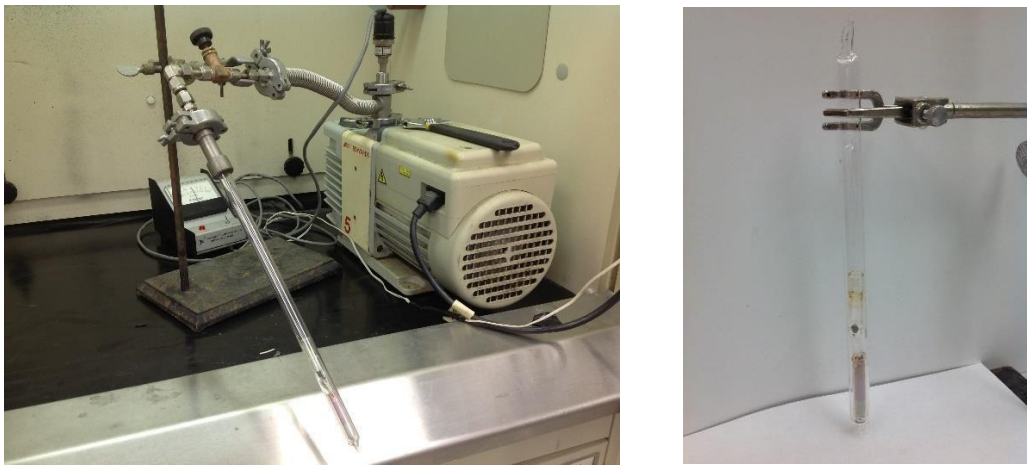

Figure 2: (left) Fused silica sealing apparatus for use with iodine-activated chemical vapor transport reactions; (right) Sealed fused silica ampoule under vacuum with reactants held in separate crucibles.

The pressure of ambient atmosphere against the vacuum in the ampoule vessel caused the slow inward collapse of the glassware, at which point the collapsed section was melted until sealed, and the two sections of tube were separated. Finally, an isolated area of the ampoule away from the powder was heated until softening to confirm that vacuum had been maintained in the vessel throughout the sealing procedure; visible as inward dimpling of the glass.

Spark Plasma Sintering

Sample powder previously reacted with titanium iodides was weighed out and loaded into an 18.75mm graphite die pre-lined with grafoil on all surfaces. The die was loaded to approximately 1000 psi in a laboratory press prior to compact the sample powder prior to loading in the SPS furnace (FCT Systeme GmbH, Rauenstein, Germany). The sintering process was conducted under vacuum, with the sample heating and pressure application schedule shown below:

$$\text{RT} \xrightarrow{\sim 100\text{K/min}} 600^\circ\text{C} \xrightarrow{\sim 120\text{K/min}} 1300^\circ\text{C} \xrightarrow[\text{dwell}]{\text{10 min.}} 1300^\circ\text{C} \xrightarrow{\sim 65\text{K/min}} \text{RT}$$

$$11\text{MPa} \longrightarrow 30\text{ MPa} \longrightarrow 30\text{ MPa} \longrightarrow 11\text{MPa} \longrightarrow 11\text{MPa}$$

The sample temperature was controlled by thermocouple to a temperature of 450°C, at which point it was controlled by a pyrometer focused on the surface of the die, up to the maximum sintering temperature of 1300°C.

Characterization and Modeling

Powder x-ray diffraction (XRD) analyses were conducted on Bruker D-2 Phaser or D-8 Advance models with zero background holders. Rietveld refinement using Topas software package (Bruker) was employed to quantify lattice parameters. Scanning electron microscopy (SEM) analyses were conducted on an FEI Quanta 200F Environmental Scanning Electron Microscope (field emission gun) or JEOL (model) equipped with secondary electron (SE) and backscattered electron (BSE) detectors and energy dispersive spectroscopy.

FactSAGE 6.4 was utilized to model equilibrium thermodynamics of isochoric and/or isothermal reactions.

Results

The following figures and descriptions summarize pertinent data obtained during the primary performance period.

X-Ray Diffraction (XRD)

XRD analyses were utilized to determine the degree of homogenization of starting materials and extent of conversion upon solid state and gas-solid reaction processing.

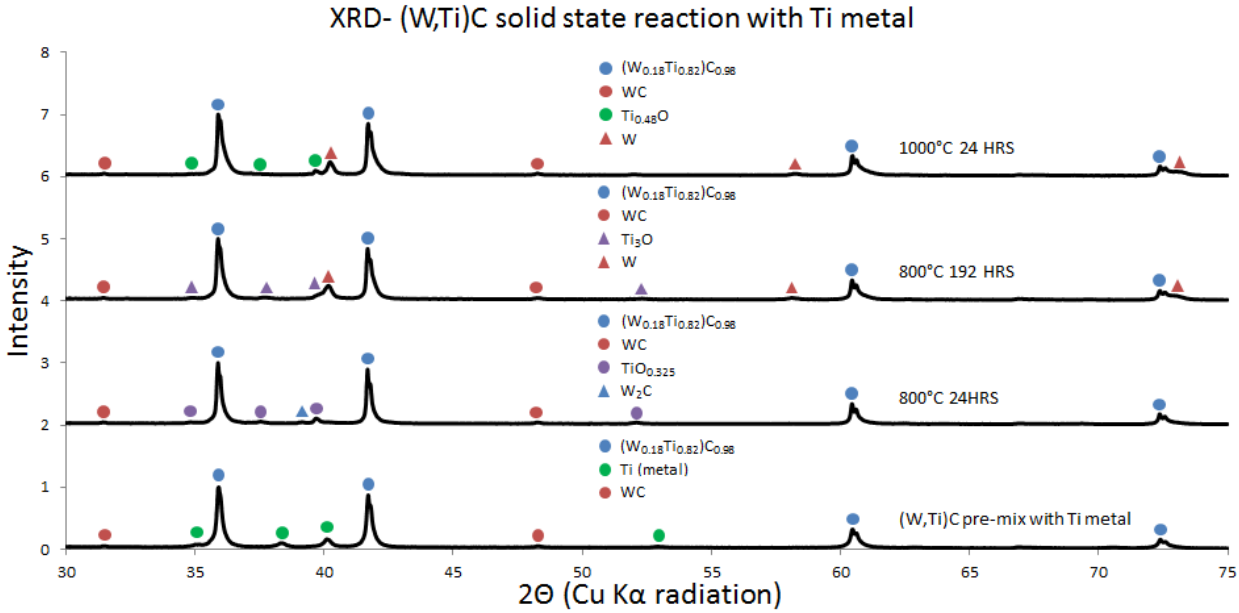

Figure 3: XRD spectra with phase identification (bottom to top): as-received mixed carbide powder showing trace WC contamination, mixed with titanium metal; post-reaction products from solid state reactions at 800°C after 24 h and 192 h; and, post-reaction products from solid state reaction at 1000°C after 24 h.

As seen in Figure 3, solid-state reacted pellets showed evidence of partial oxidation. Unlike gas-solid reactions conducted in evacuated and sealed ampoules (Figure 4), solid-state reactions were conducted within a retort furnace under an inert cover gas. It is believed that residual oxygen in the ultra-high purity argon cylinder is the cause of the oxidation. Future efforts will incorporate gas purifiers to the inert gas lines to avoid repeat of this problem.

The mixed titanium-tungsten carbide powder was selected for bulk consolidation trials via spark plasma sintering (SPS) primarily owing to its commercial availability, circumventing the need to scale up reactant powder production. As shown in Figure 5, only a minimal amount of tungsten returned to solid solution during SPS consolidation. Incorporation of tungsten sheet as a carbon diffusion barrier in contact with the graphite die was found to be unnecessary, as the thin re-carbidized surface could easily be removed via surface grinding and polishing.

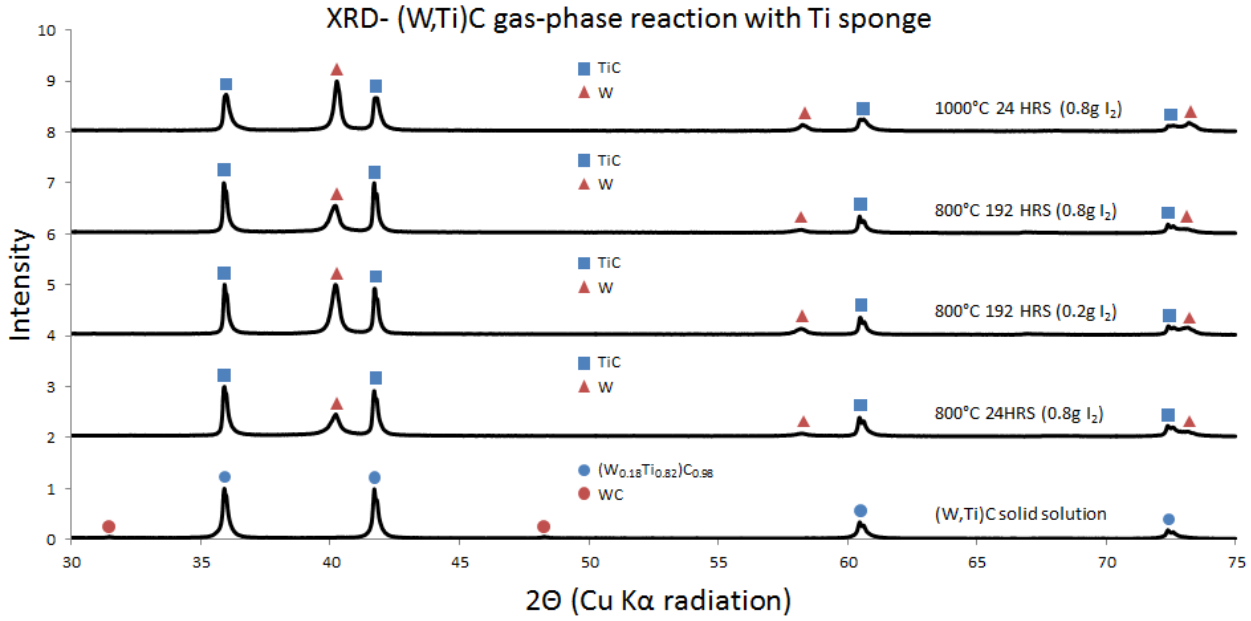

Figure 4: XRD spectra with phase identification (bottom to top): as-received mixed carbide powder showing trace WC contamination; post-reaction products from gas-solid reactions at 800°C after 24 h and 192 h and with varying amount of halide activator; and, post-reaction products from gas-solid reaction at 1000°C after 24 h.

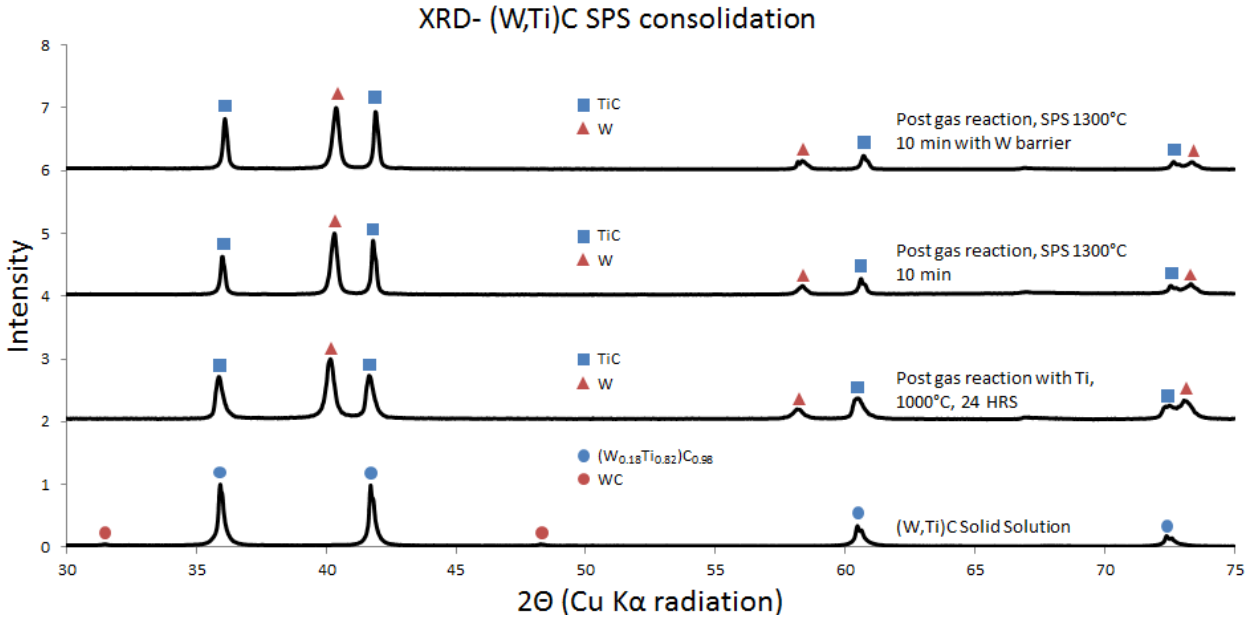

Figure 5: XRD spectra with phase identification (from bottom to top): as-received mixed carbide powder showing trace WC contamination; post-reaction products from gas-solid reaction at 1000°C after 24 h; and, phases present upon spark plasma sintering of the powders produced via gas-solid reaction at 1000°C after 24 h with and without tungsten barrier layers between the die and powders.

Preliminary screening trials of mixed titanium-niobium carbides reacted in solid state with titanium metal failed to induce precipitation of a second phase, as shown in Figure 6 below. As a result, this carbide system was de-prioritized and not investigated further.

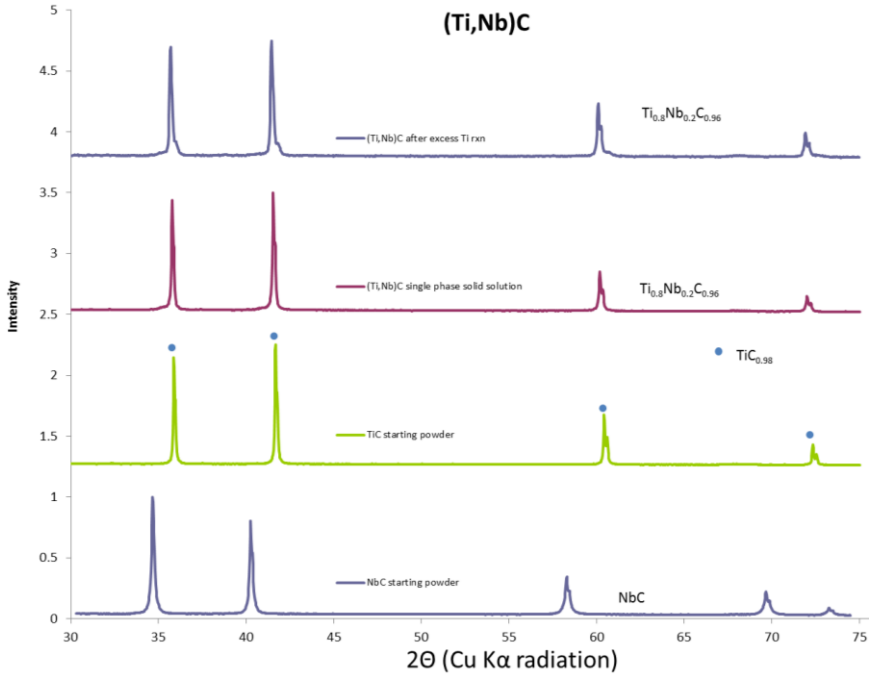

Figure 6: XRD spectra with phase identification (from bottom to top): as-received carbide powders; mixed carbide solid solution formed via high temperature homogenization treatment; and, post-reaction product from solid state reaction.

Titanium-niobium nitride powders were solid solutionized and subsequently reacted with titanium metal in the solid state or via halide intermediates within sealed ampoule, as shown in the figure below.

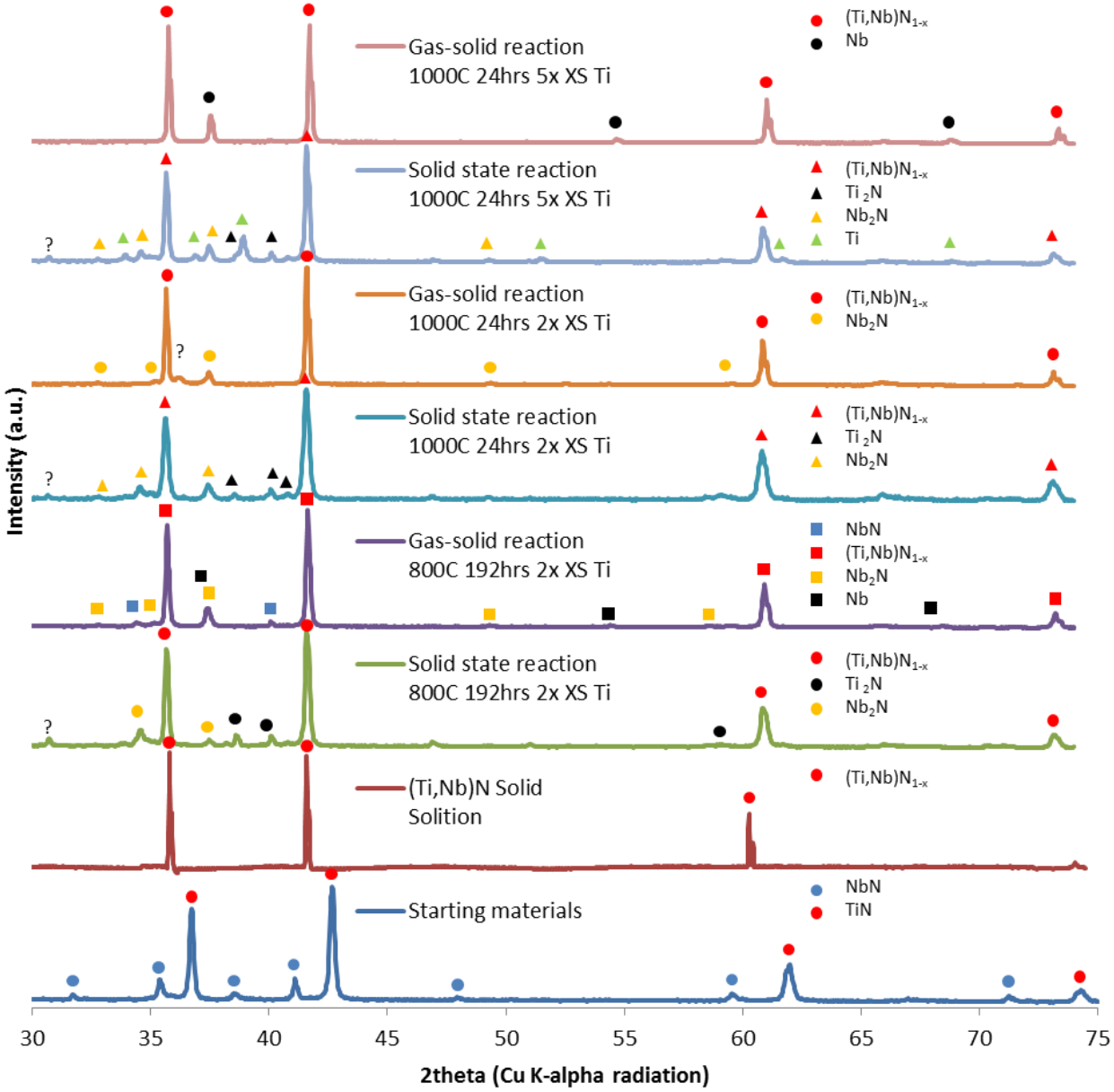

Figure 7: XRD spectra with phase identification (from bottom to top): as-received nitride powders; mixed nitride solid solution formed via homogenization heat treatment; post-reaction products from solid-solid reaction with 2:1 titanium reactant excess at 800°C after 192 h; post-reaction products from gas-solid reaction with 2:1 titanium reactant excess at 800°C after 192 h; post-reaction products from solid-solid reaction with 2:1 titanium reactant excess at 1000°C after 24 h; post-reaction products from gas-solid reaction with 2:1 titanium reactant excess at 1000°C after 24 h; post-reaction products from solid-solid reaction with 5:1 titanium reactant excess at 1000°C after 24 h; post-reaction products from gas-solid reaction with 5:1 titanium reactant excess at 1000°C after 24 h.

Titanium-niobium diboride powders were synthesized, but significant carbide contamination was observed after 2100°C heat treatment in a graphite-element vacuum furnace. Subsequent reactions in the solid-state with varying amounts of excess titanium reactant did not indicate any significant phase transformations aside from minor oxidation from the furnace atmosphere.

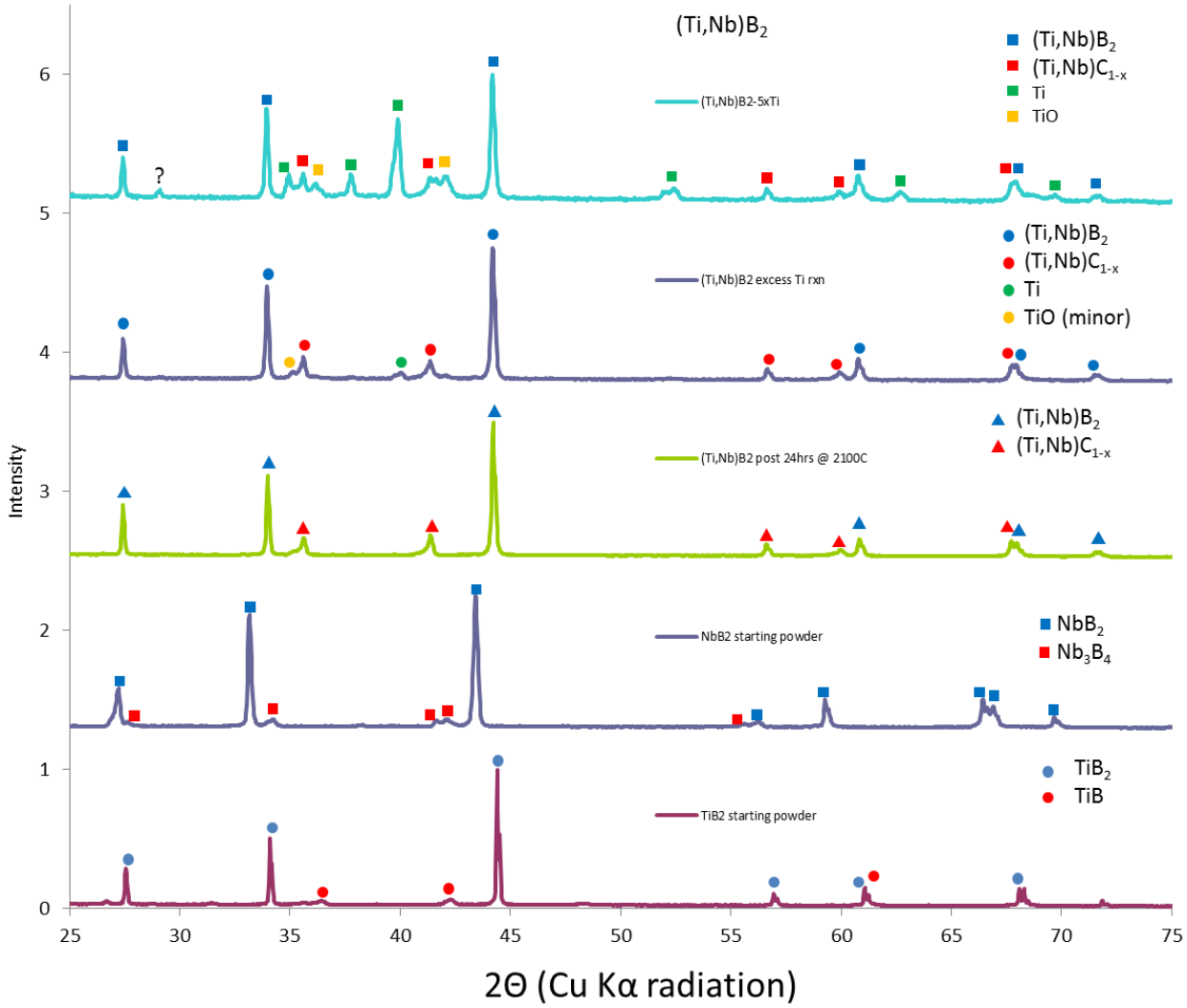

Figure 8: XRD spectra with phase identification (from bottom to top): as-received titanium boride powder showing minor graphite contamination; as-received niobium boride powder showing second phase contamination; mixed boride solid solution formed via high temperature (2100°C) homogenization treatment; post-reaction products from solid state reaction with 2:1 reactant titanium excess at 1000°C for 24 h; and, post-reaction products from solid state reaction with 5:1 reactant titanium excess at 1000°C for 24 h.

Titanium-niobium oxide powders with rutile structure were successfully synthesized. Subsequent gas-solid and solid-state reactions showed the formation of numerous suboxide phases, as seen in the figure below:

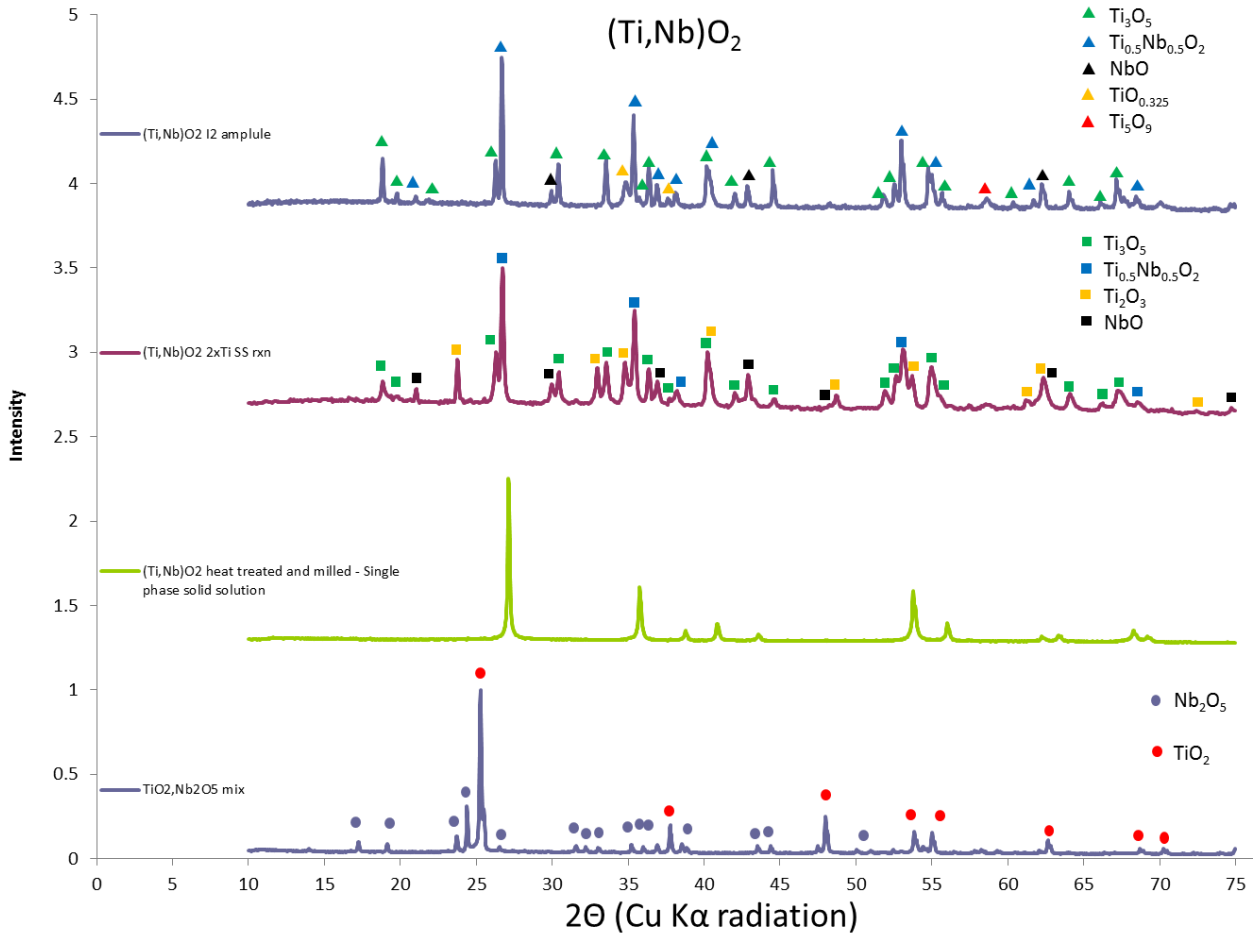

Figure 9: XRD spectra with phase identification (from bottom to top): as-received oxide powders; mixed oxide solid solution formed via high temperature homogenization treatment; post-reaction product from solid state reaction; and, post-reaction products from chemical vapor transport method.

Corundum aluminum-chromium oxide solid solution was successfully synthesized via ceramic powder processing and heat treatment. However, no appreciable reaction could be observed upon solid state or halide mediated gas-solid reaction at 1000°C for 24 hours.

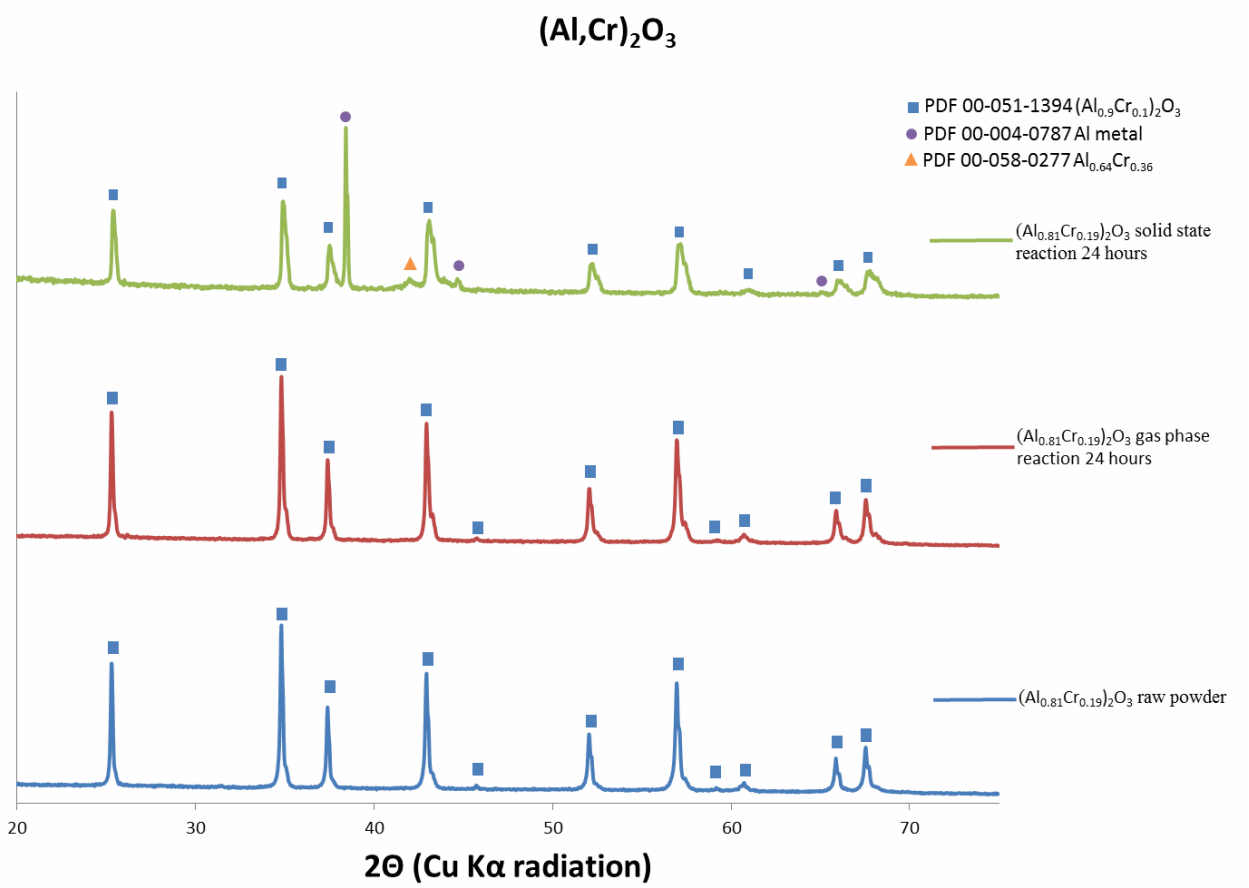

Figure 10: XRD spectra with phase identification (from bottom to top): mixed oxide solid solution formed via high temperature homogenization treatment; post-reaction products from chemical vapor transport method; and, post-reaction product from solid state method.

Scanning Electron Microscopy (SEM)

SEM observation has been employed to qualitatively evaluate precipitate morphology in recovered reaction products from both gas-solid and solid-state reactions. Due to the availability of (Ti,W)C starting material, this system was the focus of SEM analysis and subsequent SPS consolidation. Internal precipitation morphology has been directly observed for the (Ti,W)C system upon gas-solid reactions with titanium iodides at 1000°C for 24 h. As seen in Figure 11, backscattered electron images of polished and ion milled particle cross-sections reveal internal precipitation morphologies ranging from discrete particulates of various shapes and sizes to lamellar structures of varying coarseness. Focused ion beam milling was conducted at The University at Buffalo with the assistance of Dr. Yueling Qin.

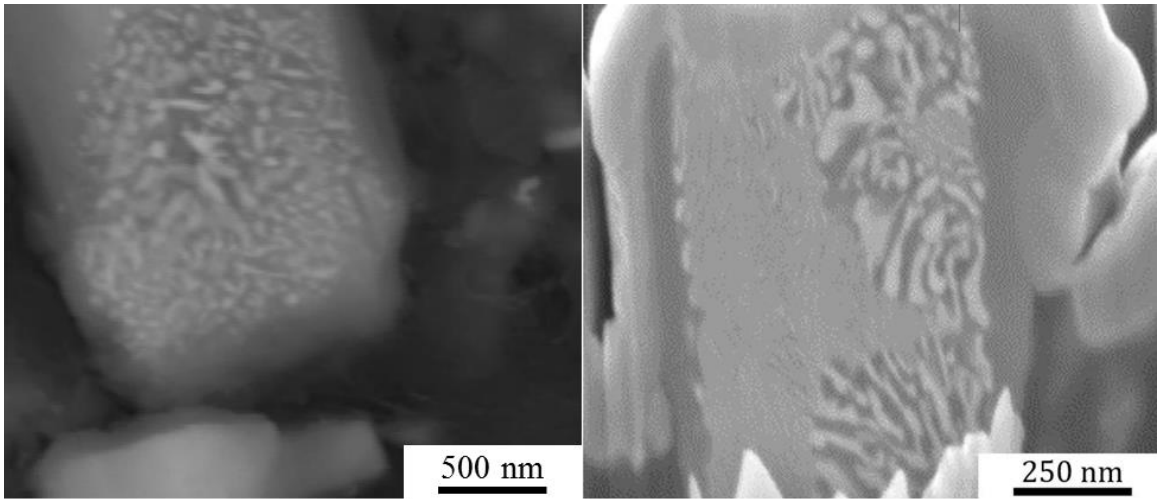

Figure 11: Backscattered electron images of (left) polished cross-sections and and (right) focused ion beam cross-sectioned particle from post-reaction products upon gas-solid reaction at 1000°C for 24 h.

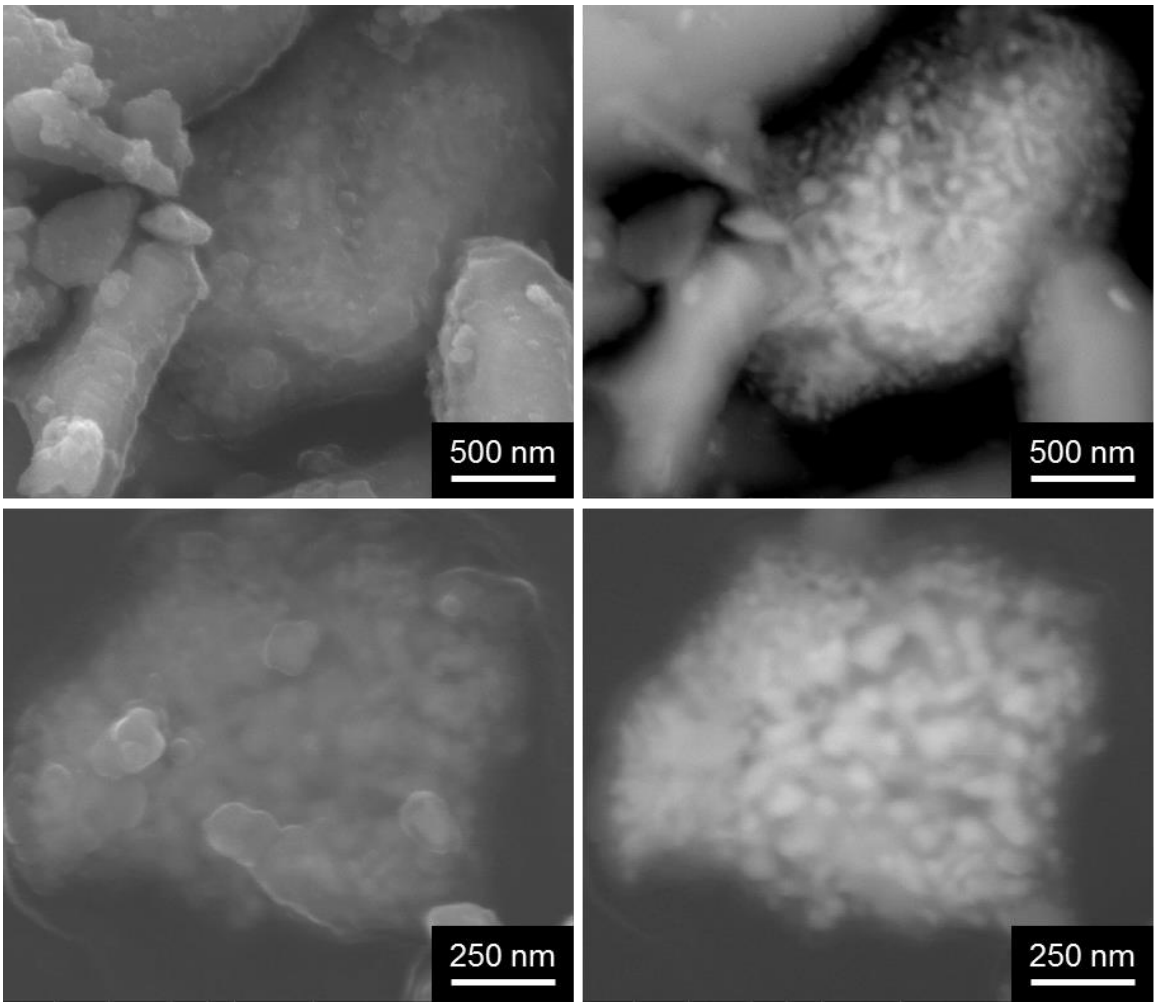

Figure 12: (Left, top and bottom) Secondary electron and (right, top and bottom) backscattered electron image pairs of selected post-reacted (Ti,W)C grains upon gas-solid reaction at 1000°C for 24 h.

The internal structure of some grains could be directly imaged via SEM without the need for particle cross-section. For example, Figure 12 features two SE/BSE SEM image pairs highlighting the presence of a thin film thought to be the gas-formed TiC layer upon an inner core comprising W nanoparticles in a TiC matrix.

Post-reacted (Ti,W)C powders upon gas-solid reaction at 1000°C for 24 h were synthesized in sufficient quantity such that the material could be pressed into dense discs via spark plasma sintering (SPS). Representative microstructures of polished cross-sections were prepared for SEM analysis (Figure 13). Bright phases are thought to correspond to tungsten, while the dark phase represents (Ti,W)C mostly depleted of its tungsten content. Contrast variation in the matrix phase is likely due to inhomogeneous distributions of tungsten from particle-to-particle. The preservation of fine tungsten precipitates is evident, along with the presence of larger (>100 nm) tungsten particles as well as (Ti,W)C grains devoid of precipitate content. No evidence of significant residual porosity was observed in SPS-consolidated specimens.

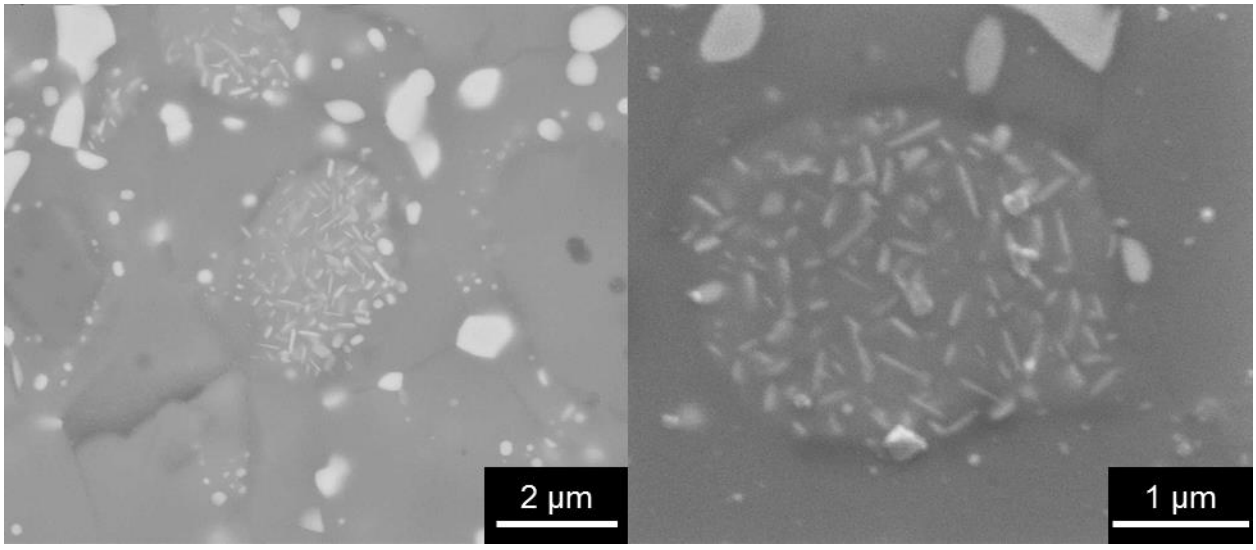

Figure 13: Backscattered electron images of SPS-consolidated gas-solid reacted (Ti,W)C powders (reacted 1000°C, 24h).

Discussion

In the following section, interpretations of results from data collected during the primary performance period are provided.

Mixed Oxide and Non-Oxide Solid Solution Ceramic Powder Processing

Synthesis of single-phase solid solution ceramic powders via traditional powder processing routes was met with mixed success. The degree of inhomogeneity with respect to stoichiometric variations and particle size distributions remains unknown and requires further analysis. Contamination from milling media is also a concern due to the abrasive nature of the ceramic phases used in this study. Future milling studies are

planned to evaluate the efficacy of steel milling media in combination with post-milling leaching procedures. Development of alternative means of powder production that increases particle-to-particle homogeneity, decreases contamination levels, and provides for greater control over crystallite and aggregate particle size distributions remains an area of high importance.

Gas-Solid Reaction Processing

Safe batch design requires careful consideration of the autogenous pressure contained within sealed fused silica ampoules. To avoid ampoule failure, total internal pressures should be limited to less than one atmosphere. For example, the figure below shows the calculated fugacities of major species contained in an ampoule for the gas-solid reactive conversion of (Ti,W)C material:

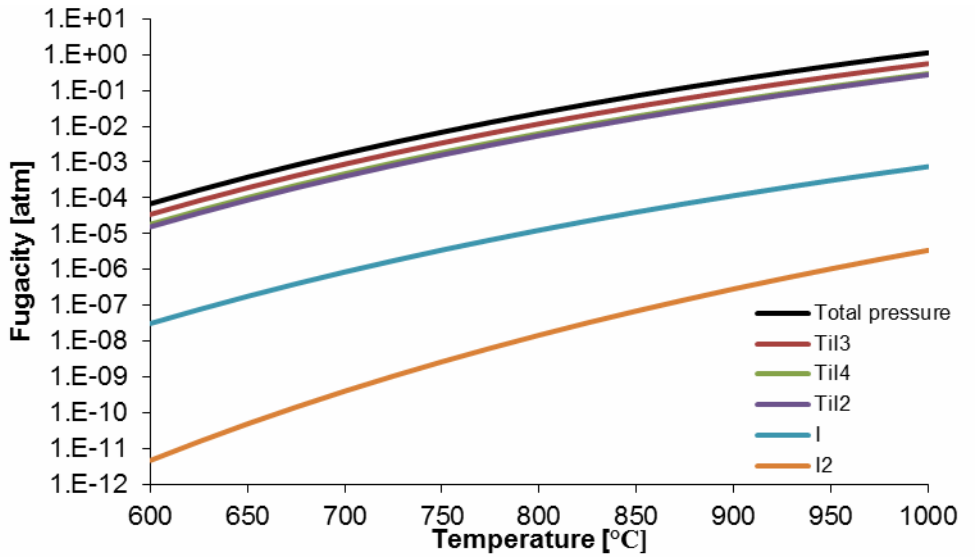

Figure 14: Isochoric (V = 17.6 cm³) gas phase composition as a function of temperature calculated using FactSAGE 6.4 for a closed system initially comprising 0.80 g iodine, 0.75 g titanium sponge, and 2.00 g ($Ti_{0.77}W_{0.23}$)C (ideal solid solution) powder.

Autogenous pressure is sensitive to batch volume and reactant amounts placed within the ampoule. Equilibrium thermodynamics predict that (Ti,W)C solid solutions will be near fully depleted of tungsten carbide content stemming from tungsten precipitation out of the supersaturated solid solution. Assuming an ideal solution model for the mixed carbide, the calculated molar composition δ of the product matrix ($Ti_\delta W_{1-\delta}$)C upon reaction with excess titanium is plotted in the figure below:

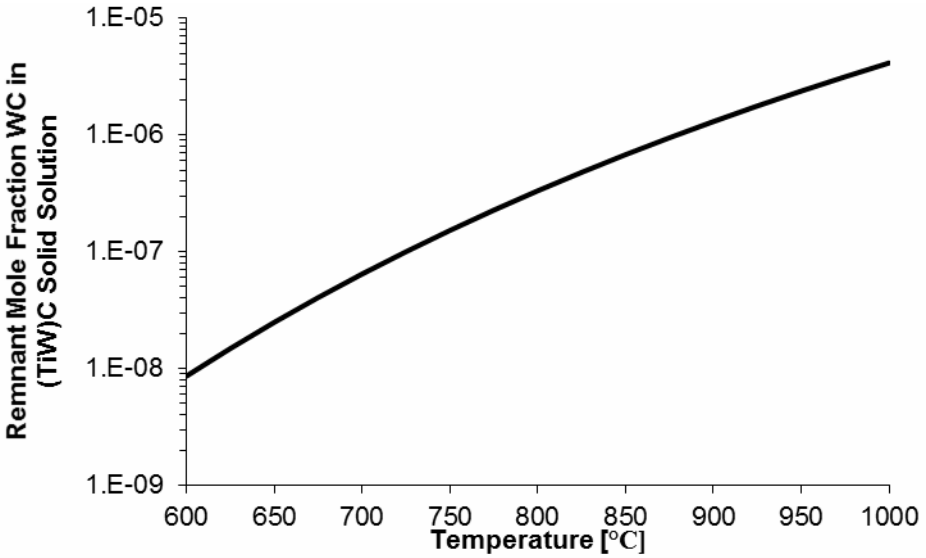

Figure 15: Equilibrium remnant mole fraction WC in (Ti,W)C upon gas-solid reaction of $(Ti_{0.77}W_{0.23})C$ with excess titanium. Calculated using FactSAGE 6.4 assuming ideal solid solution behavior of the mixed carbide phase.

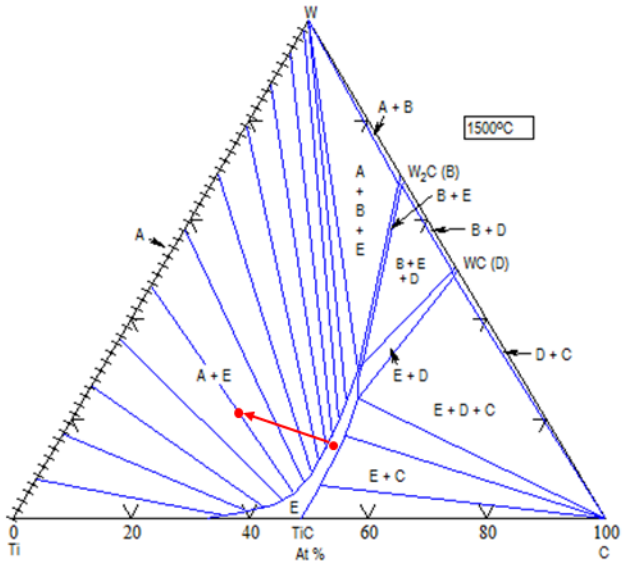

The starting composition of the mixed tungsten-titanium carbide and the composition upon complete reaction are chosen such that the system phase equilibria shift from the single phase region to the two phased region shown on the isothermal ternary phase diagram shown at left.

Figure 16: C-Ti-W ternary phase diagram, isothermal section at 1500°C. Phase diagram from E. Rudy. "Constitution of ternary titanium-tungsten-carbon alloys." J. Less-Common Met., 33.2 (1973): 245-273.

Quantitative Rietveld XRD analyses of reaction products were performed in order to assess the extent of reactive conversion as a function of process parameters. As shown in Figure 17, gas-solid reactions showed greater extents of conversion as compared to solid-state reaction samples for the same processing conditions. The relatively slow kinetics of solid-state conversion were attributable to poor contact between the solid solution and metal reactants. Despite its relative efficiency, gas-solid kinetics were insufficiently rapid to induce full theoretical yield within the chosen process parameter space. Future research activities may attempt to modify mass transport conditions from fixed bed to rotary or fluidized bed configurations to greatly improve both conversion kinetics and uniformity of reaction products.

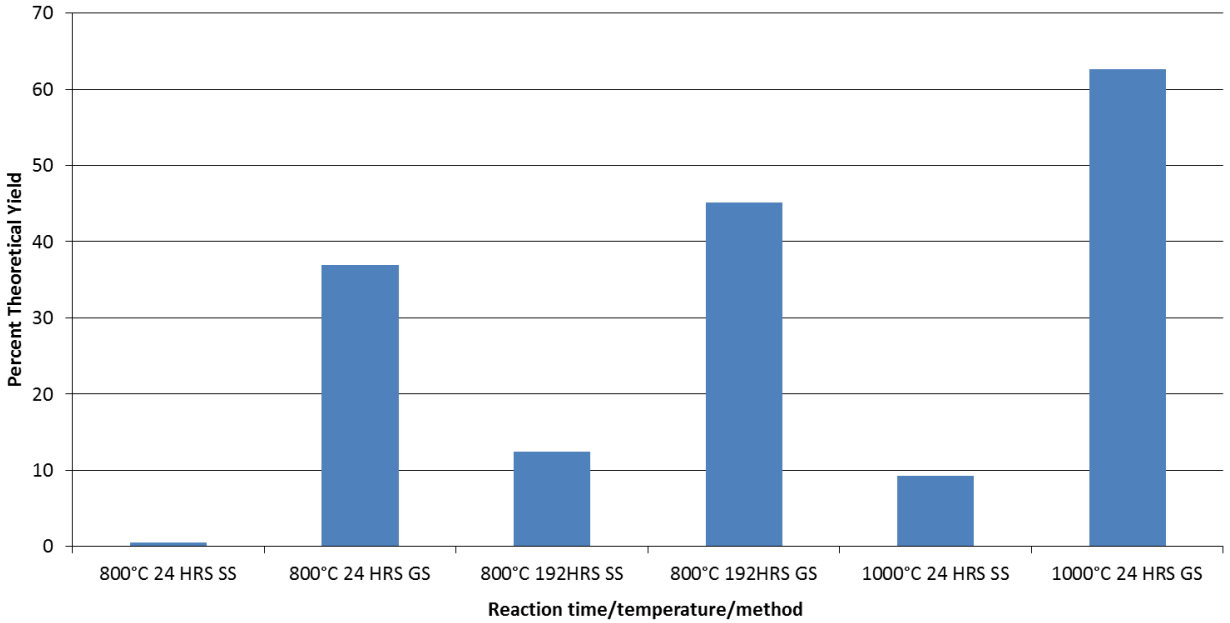

Figure 17: Extent of reactive conversion of ($Ti_{0.77}W_{0.23}$)C into TiC and W for gas-solid and solid-state reactions at the specified process conditions.

Poor inter-particle connectivity could theoretically be remedied using any method to uniformly coat solid solution reactant powders with controlled amounts of metallic reactants. However, if the starting powders have a wide size distribution, then it may not be possible to empirically optimize coating thicknesses, leading to a wide range of compositional variation on a particle-to-particle basis. The gas-solid reaction paradigm utilized in this study circumvents this disadvantage by avoiding direct deposition of metal from the gas phase altogether. Instead, the gas phase undergoes heterogeneous reaction with super-saturated carbon from the solid solution that has outwardly diffused to the gas-solid interface, resulting in a reaction-formed carbide deposit. As evidenced via XRD, no metallic phase deposited as coatings on the powder can be identified.

The occurrence of internal precipitation morphology upon gas-solid reaction of ($Ti_{0.77}W_{0.23}$)C is likely due to much greater carbon diffusivity as compared to titanium and tungsten diffusivities within the titanium carbide host lattice. The present author speculates observed variability in product morphology to be attributable mainly to inhomogeneous starting materials. That the starting powder is not perfectly homogeneous can be readily seen upon inspection of XRD spectra that show the presence of WC contamination as well as asymmetric peak broadening (Figure 18) that is indicative of a series of WC-deficient solid solutions. Reactant particles rich in WC content would be more likely to produce the larger (> 500 nm) observed standalone tungsten particles, as the attendant volume change upon reaction would be expected to greatly exceed the failure strain of the matrix material resulting in microcracking and possibly grain fracture. Fracture surfaces would then allow rapid transport of tungsten via gas and solid phase mechanisms, promoting coarsening to sizes far exceeding those observed where intragranular morphology was retained.

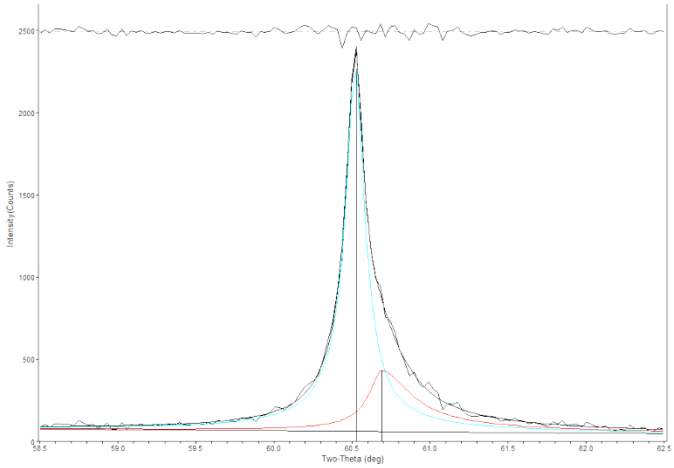

Figure 18: Deconvoluted [220] reflection after algorithmic removal of Cu-Kα2 signal in Jade 8 (Materials Data Inc.).

While reactive conversion in the (Ti,W)C system and subsequent SPS-consolidation has met with early success, the $(Al,Cr)_2O_3$ corundum system has not yet been demonstrated to produce internal precipitation morphologies, perhaps a consequence of greater diffusivities for aluminum and chromium as compared to oxygen within the host lattice at the processing temperature of 1000°C. Studies of this system are further complicated by the occurrence of Al-Cr intermetallics and a non-volatile CrI_2 solid that can sequester iodine and inhibit gas phase transport of aluminum. Despite these complications, continued study of this system is recommended for several reasons. First, equilibrium thermodynamics indicate that the solid solution may virtually be fully depleted of chromium content upon complete reaction, resulting in precipitation of chromium or a variety of intermetallic species (Figures 19 and 20).

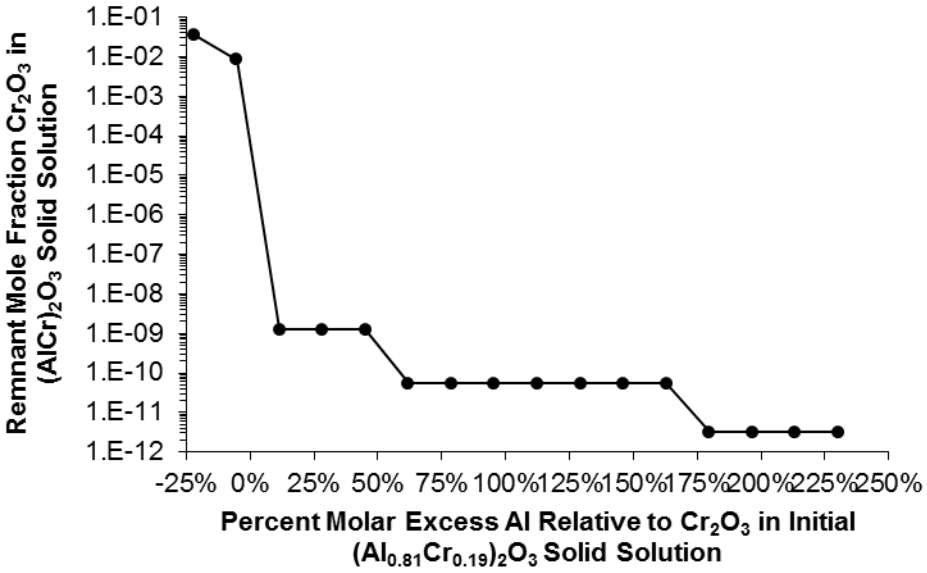

Figure 19: Equilibrium remnant mole fraction Cr_2O_3 in $(AlCr)_2O_3$ upon chemical vapor transport reaction of $(Al_{0.81}Cr_{0.19})_2O_3$ with excess aluminum. Calculated using FactSAGE assuming ideal solid solution behavior of the mixed carbide phase.

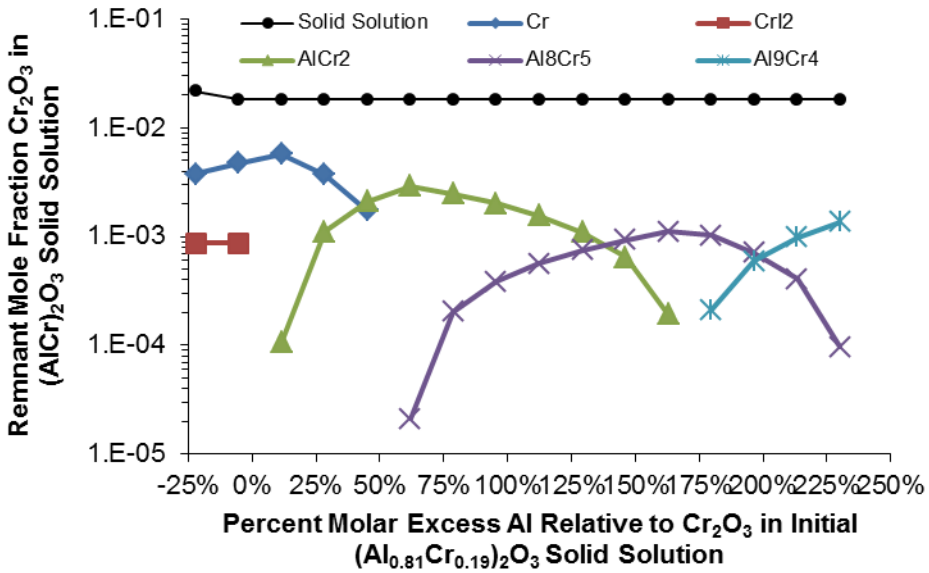

Figure 20: Solid phase constitution as a function of percent molar excess aluminum relative to chromia in mixed oxide solid solution. Calculated using FactSAGE 6.4 for an isothermal (T = 1000°C), isochoric (V = 17.6 cm³) system comprising fixed amounts of iodine (0.22 g) and $(Al_{0.81}Cr_{0.19})_2O_3$ powder (2.00 g).

Second, phase decomposition in the $(Al,Cr)_2O_3$ system has been studied by previous researchers utilizing flowing hydrogen as a reducing agent at temperatures exceeding 1500°C. The system represents a prototype case study for comparing the use of metallic reducing agents transported via the gas phase as compared to gaseous reducing agents that merely control the oxygen fugacity at the surface of the reacting particle. Not only do metallic reducing agents provide greater thermodynamic driving forces owing to the concomitant formation of a condensed metal oxide typically characterized by a highly negative standard Gibbs free energy of formation, but this second phase, when epitaxially deposited upon a monocrystalline reactant grain, can enable the formation of pseudo-intragranular reinforcement morphology (Figure 1).

Designing reaction systems for the promotion of internal precipitation morphologies remains difficult due to sparse diffusion data in single crystals at modest temperatures for the ceramic systems under study. It is important to locate single crystal data versus bulk, polycrystalline data so as to avoid errant conclusions drawn from the existence of rapid grain boundary diffusion and other short circuit diffusion pathways. Unfortunately, in the absence of this data and in means to generate this data in the laboratory, a semi-empirical approach to reactant system-dependent processing parameter space remains necessary.

Not yet discussed are the results from the reaction of the $(Ti,Nb)B_2$ and $(Ti,Nb)O_2$ systems and the (Ti,Nb)C system. Due to the complexity of the phase assemblage in the reaction products of the diboride and oxide systems, until such time that a process model can be validated these systems are not recommended for further study. Due to the success with the surrogate (Ti,W)C system – which is a commercially available

material system – it seems redundant to study the (Ti,Nb)C system. There is, however, one important distinction between these two mixed carbide solid solutions. Namely, the homogeneity range on the carbon deficient side of the phase diagrams differ greatly among the Group IV, V, and VI carbides, decreasing as one moves to the right on the periodic table. As a result, the (Ti,W)C displays only limited carbon nonstoichiometries as compared to the (Ti,Nb)C system. Indeed, a 2:1 molar excess of titanium with respect to niobium did not result in any reaction in solid-state pellet studies. The present author speculates that further increases to the titanium excess sufficient to cross into the two-phase field in the ternary Ti-Nb-C system would be borne out by additional trials.

In summary, (Ti,W)C has been demonstrated to undergo selective metallothermal reactions to produce W + TiC nanocomposite particles. For the first time, selective gas-solid reactions with both oxide and non-oxide ceramic solid solutions have been shown to produce analogous reaction products as compared to solid-state reactions, including internal precipitation morphologies in well-behaved systems. Further, nanocomposite powders can be SPS-consolidated with full retention of nanostructural features.

Future Outlook and Recommendations

The successful demonstration of selective metallothermal gas-solid reactions with solid solution ceramic powders represents a significant advancement in processing science. Under certain conditions, internal precipitation morphologies can result in a pseudo-intragranular microstructure that may circumvent issues surrounding the synthesis of ceramic nanocomposites with tailorable microstructures. The latter feature is especially important from a basic science standpoint when attempting to elucidate strengthening and toughening mechanisms in this class of materials. Additional efforts in several key areas are recommended:

- Identifying ways to improve the quality of starting materials, especially with respect to chemical homogeneity and monocrystalline character;

- Developing morphological maps as functions of temperature, time, and composition to better understand reduction pathways and their effects on microstructure;

- Exploring additional oxide and non-oxide systems exemplified by ternary systems absent intermetallics and sub-valent species and that feature rapid diffusion of the non-metal constituent;

- Reaction processing scale up; and,

- Mechanical properties testing of bulk consolidated materials.

References

[1] Anthony G. Evans. "Perspective on the Development of High-Toughness Ceramics." *J. Am. Ceram. Soc.* 73.2 (1990): 187-206.

[2] Paul F. Becher. "Microstructural Design of Toughened Ceramics." *J. Am. Ceram. Soc.* 74.2 (1991): 255-269.

[3] S.M. Wiederhorn. "Brittle fracture and toughening mechanisms in ceramics." *Ann. Rev. Mater. Sci.* 14 (1984): 373-403.

[4] P.A. Mataga. "Deformation of crack-bridging ductile reinforcements in toughened brittle materials." *Acta metall.* 37.12 (1989): 3349-3359.

[5] V.D. Krstic. "On the fracture of brittle-matrix/ductile-particle composites." *Phil. Mag. A* 48.5 (1983): 695-708.

[6] Junhong Zhao, Laura C. Stearns, Martin P. Harmer, Helen M. Chan, Gary A. Miller, and Robert E. Cook. *"*Mechanical behavior of alumina-silicon carbide *'*nanocomposites*'."* *J. Am. Ceram. Soc.* 76.2 (1993): 503-510.

[7] Brian Derby. *"*Ceramic nanocomposites: mechanical properties.*"* *Current Op. Sol. St. Mater. Sci.* 3 (1998): 490-495.

[8] H. Wu. *"*Understanding residual stresses and fracture toughness in ceramic nanocomposites.*"* Residual Stresses in Composite Materials. Ed. Mahmood M. Shokrieh. Cambridge: Woodhead Publishing, 2014. 256-292.

[9] Koichi Niihara. "New Design Concept of Structural Ceramics -Ceramic Nanocomposites-." *J. Ceram. Soc. Japan* 99.10 (1991): 974-982.

[10] Tatsuki Ohji, Young-Keun Jeong, Yong-Ho Choa, and Koichi Niihara. "Strengthening and Toughening Mechanisms of Ceramic Nanocomposites." *J. Am. Ceram. Soc*. 81.6 (1998): 1453-1460.

[11] Minoru Taya, S. Hayashi, Albert S. Kobayashi, and H.S. Yoon. "Toughening of a Particulate-Reinforced Ceramic-Matrix Composite by Thermal Residual Stress." *J. Am. Ceram. Soc.* 73.5 (1990): 1382-1391.

[12] W.H. Tuan and R.J. Brook. "The Toughening of Alumina with Nickel Inclusions." *J. Euro. Ceram. Soc.* 6 (1990): 31-37.

[13] Xudong Sun and Julie Yeomans. "Optimization of a Ductile-Particle Toughened Ceramic." *J. Am. Ceram. Soc.* 79.10 (1996): 2705-2717.

[14] J.A. Yeomans. "Ductile particle ceramic matrix composites - Scientific curiosities or engineering materials?" *J. Euro. Ceram. Soc*. 28 (2008): 1543-1550.

[15] Xudong Sun and J.A. Yeomans. "Ductile Phase Toughened Brittle Materials." *J. Mater. Sci. Technol.* 12 (1996): 124-134.

[16] Xudong Sun and J.A. Yeomans. "Microstructure and fracture toughness of nickel particle toughened alumina matrix composites." *J. Mater. Sci.* 31 (1996): 875-880.

[17] Fazil Erdogan and Paul F. Joseph. "Toughening of Ceramics through Crack Bridging by Ductile Particles." *J. Am. Ceram. Soc.* 72.2 (1989): 262-270.

[18] Giuseppe Pezzotti and Wolfgang H. Muller. "Strengthening mechanisms in Al_2O_3/SiC nanocomposites." *Computational Mater. Sci.* 22 (2001): 155-168.

[19] Honglai Tan and Wei Yang. "Toughening mechanisms of nano-composite ceramics." *Mech. Mater.* 30 (1998): 111-123.

[20] Hideo Awaji, Seong-Min Choi, and Eisuke Yagi. "Mechanisms of toughening and strengthening in ceramic-based nanocomposites." *Mech. Mater.* 34 (2002): 411-422.

[21] Luca Paolo Ferroni and Giuseppe Pezzotti. "Evidence for Bulk Residual Stress Strengthening in Al_2O_3/SiC Nanocomposites." *J. Am. Ceram. Soc.* 85.8 (2002): 2033-2038.

[22] "Nanocomposites." Handbook of Nanophase and Nanostructured Materials. Volume 4: Materials Systems and Applications (II). Ed. Zhong Lin Wang, Yi Liu, and Ze Zhang. New York: Kluwer Academic/Plenum Publishers, 2002. 85-110.

[23] Martin Sternitzke. "Review: Structural Ceramic Nanocomposites." *J. Euro. Ceram. Soc.* 17 (1997): 1061-1082.

[24] Jose S. Moya, Sonia Lopez-Esteban, and Carlos Pecharroman. "The challenge of ceramic/metal microcomposites and nanocomposites." *Prog. Mater. Sci.* 52 (2007): 1017-1090.

[25] Seong-min Choi, Sawao Honda, Shinobu Hashimoto, and Hideo Awaji. "Intra-type nanocomposites for strengthened and toughened ceramic materials." Characterization, Design, and Processing of Nanosize Powders and Nanostructured Materials. Ed. Kevin G. Ewsuk and Yury Gogotsi. Hoboken, New Jersey: John Wiley & Sons, Inc. 2006. 173-180.

[26] Youren Xu, Avigdor Zangvil, and Albert Kerber. "SiC Nanoparticle-Reinforced Al_2O_3 Matrix Composites: Role of Intra- and Intergranular Particles." *J. Euro. Ceram. Soc.* 17 (1997): 921-928.

[27] S. Kovalev, T. Ohji, Y. Yamauchi, and M. Sakai. "Grain boundary strength in non-cubic ceramic polycrystals with misfitting intragranular inclusions (nanocomposites)." *J. Mater. Sci.* 35 (2000): 1405-1412.

[28] Xudong Sun, Ji-Guang Li, Shiwen Guo, Zhimeng Xiu, Kai Duan, and Xiao Zhi Hu. "Intragranular Particle Residual Stress Strengthening of Al_2O_3-SiC Nanocomposites." *J. Am. Ceram. Soc.* 88.6 (2005): 1536-1543.

[29] Alan Piciacchio, Sang-Ho Lee, and Gary L. Messing. "Processing and Microstructure Development in Alumina-Silicon Carbide Intragranular Particulate Composites." *J. Am. Ceram. Soc.* 77.8 (1994): 2157-2164.

[30] A.J. Winn and R.I. Todd. “Microstructural requirements for alumina-SiC nanocomposites.” *Brit. Ceram. Trans.* 98.5 (1999): 219-224.

[31] E. Ustundag, R. Subramanian, R. Dieckmann, and S.L. Sass. "In situ formation of metal-ceramic microstructures in the Ni-Al-O system by partial reduction reactions." *Acta metall. mater.* 43.1 (1995): 383-389.

[32] E. Ustundag, R. Subramanian, R. Vaia, R. Dieckmann, and S.L. Sass. "In situ formation of metal-ceramic microstructures, including metal-ceramic composites, using reduction reactions." *Acta metall. mater.* 41.7 (1993): 2153-2161.

[33] R. Subramanian, E. Ustundag, S.L. Sass, and R. Dieckmann. "In-situ formation of metal-ceramic microstructures by partial reduction reactions." *Solid St. Ionics* 75 (1995): 241-255.

[34] C.A. Handwerker, T.J. Foecke, J.S. Wallace, U.R. Kattner, and R.D. Jiggets. "Formation of alumina-chromia-chromium composites by a partial reduction reaction." *Mater. Sci. Eng.* A195 (1995): 89-100.

[35] Hermann Schmalzried and Monika Backhaus-Ricoult. "Internal solid state reactions." *Prog. Solid St. Chem.* 22 (1993): 1-57.

[36] Kirk A. Rogers and Kevin P. Trumble. "Effect of reduction temperature on internal reduction microstructures." *Scripta Mater.* 39.1 (1998): 103-108.

[37] Monika Backhaus-Ricoult, Serge Hagege, Aurelie Peyrot, and Patrick Moreau. "Internal Reduction of Chromium-Doped alpha-Alumina." *J. Am. Ceram. Soc.* 77.2 (1994): 423-430.

[38] David W. Lipke, Yunshu Zhang, Ye Cai, and Kenneth H. Sandhage. “Intragranular Tungsten/Zirconium Carbide Nanocomposites via a Selective Liquid/Solid Displacement Reaction.” *J. Am. Ceram. Soc.* 95 (2012): 2769-2772.

[39] David W. Lipke and Kenneth H. Sandhage. “Intragranular Nanocomposites via Internal Reduction of Carbide Solid Solutions.” *ECS Trans.* 50.14 (2013): 85- 93.